
Article:
Lio, W.H. orcid.org/0000-0002-3946-8431, Jones, B. and Rossiter, J.A. orcid.org/0000-0002-1336-0633 (2017) Preview predictive control layer design based upon known wind turbine blade-pitch controllers. Wind Energy. ISSN 1095-4244

https://doi.org/10.1002/we.2090

WIND ENERGY
Wind Energ. 2010; **00**:1–19
DOI: 10.1002/we

RESEARCH ARTICLE

Predictive control layer design on a known output-feedback compensator for wind turbine blade-pitch preview control

W. H. Lio, B. Ll. Jones and J. A. Rossiter

Department of Automatic Control and Systems Engineering, The University of Sheffield, Sheffield, S1 3JD, U.K.

ABSTRACT

The use of upstream wind measurements has motivated the development of blade-pitch preview controllers to improve rotor speed tracking and structural load reduction beyond that achievable via conventional feedback control. Such preview controllers, typically based upon model predictive control (MPC) for its constraint handling properties, alter the closed-loop dynamics of the existing blade-pitch feedback control system. This can result in a deterioration of the robustness properties and performance of the existing feedback control system. Furthermore, performance gains from utilising the upcoming real-time measurements cannot be easily distinguished from the feedback control, making it difficult to formulate a clear business case for the use of preview control. Therefore, the aim of this work is to formulate a modular MPC layer on top of a given output feedback blade-pitch controller, with a view to retaining the closed-loop robustness and frequency-domain performance of the latter. We derive a key result that proves that the proposed modular MPC layer handles real-time advance measurements and impacts the existing closed-loop system if and only if constraints are violated. The separate nature of the proposed controller structure enables clear and transparent quantification of the benefits gained by using preview control, beyond that of the underlying feedback controller. This is illustrated by results obtained from high-fidelity closed-loop turbine simulations, showing the performance comparison between a nominal feedback controller and an additional MPC-based preview controller. The proposed control scheme incorporating knowledge of the oncoming wind and constraints achieved significant 43% and 30% reductions in the rotor speed and flap-wise blade moment standard deviations, respectively. Additionally, the chance of constraint violations on the rotor speed decreased remarkably from 2.15% to 0.01%, compared to the nominal controller.

KEYWORDS

model predictive control; preview control; feed-forward control; blade-pitch control

Correspondence
W. H. Lio, Department of Automatic Control and Systems Engineering, The University of Sheffield, Sheffield, S1 3JD, U.K.
E-mail: w.h.lio@sheffield.ac.uk

Received . . .

1. INTRODUCTION

The rotors and structural components of large wind turbines are subjected to unsteady and intermittent aerodynamic loads from the wind. Such loads can cause the rotational speed of the rotors and power generation to exceed the design specifications and also lead to fatigue damage to key turbine structural components, resulting in a reduction in turbine lifetime. Most modern megawatt wind turbines are equipped with blade-pitch controllers for achieving turbine speed regulation. In addition, an increasing number of large wind turbines are beginning to exploit the adjustment of blade pitch angle to attenuate unbalanced loads on the rotors. These two strategies are commonly known as: (i) collective pitch control (CPC), whose role is to regulate rotor speed by adjusting the pitch angle of each blade by an identical amount, and (ii) individual pitch control (IPC), which provides an additional pitch angle demand signal, typically in response to measurements of flap-wise blade root bending moment, to mitigate the effect of unsteady loads on the rotor (e.g. [1–3]). Typical CPC and IPC control methods rely on feedback measurements, and given the large inertia of the rotor, the effectiveness of feedback compensation is inherently limited. Consequently, this motivates the potential uses of real-time advance measurement of the wind conditions for feed-forward control design in wind turbines.

Prepared using weauth.cls [Version: 2010/06/17 v1.00]

In recent years, a growing body of research has emerged, seeking to utilise real-time measurement of the approaching wind field from sensing devices for feed-forward design to further improve the performance of blade pitch control systems. Early adoption of feed-forward control in wind turbines that focused on turbine speed regulation was reported by Kodama et al. [4], in which the feed-forward control strategy was based on the hub-height wind measurement taken 40 metres in front of the rotor by an anemometer on a free standing tower. Light detection and ranging (LIDAR) devices, employed by Harris et al. [5] and numerous subsequent authors (e.g. [6–8]), demonstrated the impact on the performance of the CPC in regulating rotor speed and mitigating tower load by exploiting preview information of the approaching wind field. Lately, a number of authors (e.g. [9–12]) investigated the use of upcoming wind measurements with IPC, aiming to attenuate unbalanced loads on the rotor and blade loads. Some studies (e.g. [10]) suggested that the use of feed-forward IPC to attenuate blade loads could increase the pitch rate activities, thus, the control design needed to take into account the pitch actuator constraints carefully. As a consequence, this motivates the use of model predictive control (MPC) for its constraint handling feature.

In general, model predictive control selects the predicted future control inputs based on the optimisation of a performance criteria subject to the need for system predictions to satisfy constraint requirements. System predictions are obtained using a mathematical model of the system as well measurements of the outputs at each sample. Many studies have adopted MPC design in wind turbines (e.g. [13–16]) and their results demonstrated the effectiveness of the MPC for handling constraints on the rotor speed and blade pitch actuators. In addition, apart from the constraint handling feature, MPC can also incorporate preview information into the control design systematically. Thus, many authors [17–21]exploited this advantage by employing MPC for preview CPC and IPC design and demonstrated the performance of preview MPC designs for turbine speed regulation and flap-wise blade load reduction. More studies regarding MPC designs in wind turbines can be found in [22, 23].

Nonetheless, the majority of preview MPC studies in wind turbines use a standard MPC approach where its shortcomings are that the robustness and closed-loop frequency-domain properties are usually not well considered in the time-domain design. As the loads on turbine blades predominately exist at the harmonics of the blade rotational frequency, thus, it is more intuitive to design a robust closed-loop feedback controller in the frequency-domain to attenuate such loads. Consequently, this work aims to bridge this gap by formulating an MPC layer based on a known robust output-feedback controller where the MPC layer handles constraints and upcoming wind measurements whilst retaining the robustness properties of the existing closed-loop. Given that the constraint handling features depend upon the predictions of the closed-loop dynamics, optimising such predictions could potentially introduce an additional feedback loop as illustrated in this work. As a consequence, the desired robustness and performance of the original closed-loop dynamics can no longer remain unchanged. Therefore, a further key focus of this paper is to investigate the conditions under which the additional layer design is separated from the original closed-loop. The separate nature of this MPC layer is important from an industry perspective, since the feed-forward control can be implemented without replacing the existing feedback controller. Furthermore, it provides a clear framework to quantify the benefits of the use of advance real-time measurements over the nominal output-feedback strategy.

The remainder of this paper is structured as follows. In Section 2, the modelling aspect of the blade pitch control problem, including model disturbance, and the detail of the nominal output feedback controller are discussed. This is followed in Section 3 by a formulation of a predictive control layer. In Section 4, the potential influence of the additional control layer design on the original feedback closed-loop dynamics is explained, and the conditions are proposed to ensure the original closed-loop dynamics are retained from the extra layer design. In Section 5, details of simulation environments and tuning of the MPC layer will be discussed. Subsequently, simulation results on a high-fidelity wind turbine under various wind cases are demonstrated, showing the benefits of deploying the proposed control layer on top of the output-feedback controller. Section 6 concludes this paper with a summary and an overview of future work.

Notation

Let $\mathbb{R}$, $\mathbb{C}$ and $\mathbb{Z}$ denote the real and complex fields and set of integers, respectively, and let $s \in \mathbb{C}$ denote a complex variable. The space $\mathcal{R}$ denotes the space of proper real-rational transfer function matrices and $k \in \mathbb{Z}$ denotes a sample variable of a discrete-time signal. Let $v^T \in \mathbb{R}^{1\times n_v}$ denote the transpose of a vector $v \in \mathbb{R}^{n_v}$ and $V^T \in \mathbb{R}^{n_y \times n_z}$ is the transpose of a matrix $V \in \mathbb{R}^{n_z \times n_y}$. The notation $\underset{\rightarrow k}{v} \in \mathbb{R}^{n_v n_p}$ denotes the future prediction sequence $\left[v_{0|k}, v_{1|k} ..., v_{n_p-1|k}\right]^T \in \mathbb{R}^{n_v n_p}$.

2. WIND TURBINE MODELING AND NOMINAL ROBUST FEEDBACK COMPENSATOR

This section gives a brief background of wind turbine modelling including model disturbances and details of the chosen robust feedback controllers that are later employed by the proposed MPC layer formulation.

Wind Energ. 2010; **00**:1–19 © 2010 John Wiley & Sons, Ltd.
DOI: 10.1002/we
Prepared using weauth.cls

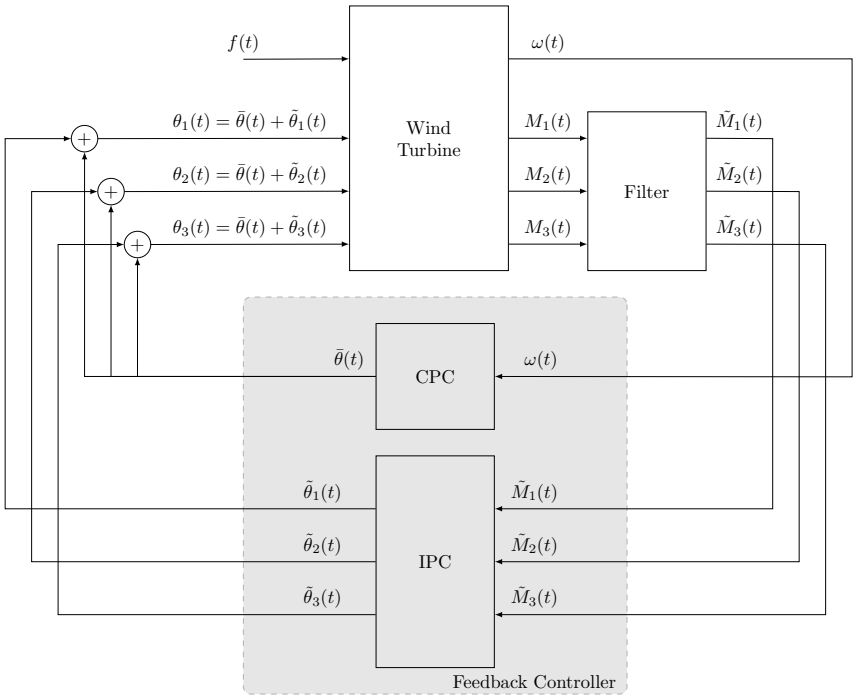

Figure 1. System architecture of a wind turbine blade-pitch control system, combining collective pitch control (CPC) and individual pitch control (IPC). The CPC regulates rotor speed while the IPC attenuates perturbations in the flap-wise root bending moments on each blade. Additional inputs to the turbine, such as wind loading and generator torque, are accounted for in the term $f(t)$.

2.1. Wind turbine modelling

A typical wind turbine blade-pitch control system architecture for above-rated conditions is shown in Figure 1. The CPC regulates the rotor speed $\omega(t)$ by adjusting the collective pitch angle signal, whilst the IPC attenuates loads by providing additional pitch signals to the collective pitch angle in response to flap-wise blade root bending moment signals. To isolate the action of the IPC from that of the CPC, it is convenient to define the pitch angles and blade moments as follows:

$$\begin{bmatrix}\theta_1^{\mathrm{c}}(t)\\ \theta_2^{\mathrm{c}}(t)\\ \theta_3^{\mathrm{c}}(t)\end{bmatrix} := \begin{bmatrix}\bar{\theta}^{\mathrm{c}}(t) + \tilde{\theta}_1^{\mathrm{c}}(t)\\ \bar{\theta}^{\mathrm{c}}(t) + \tilde{\theta}_2^{\mathrm{c}}(t)\\ \bar{\theta}^{\mathrm{c}}(t) + \tilde{\theta}_3^{\mathrm{c}}(t)\end{bmatrix}, \quad \begin{bmatrix}M_1(t)\\ M_2(t)\\ M_3(t)\end{bmatrix} := \begin{bmatrix}\bar{M}(t) + \tilde{M}_1(t)\\ \bar{M}(t) + \tilde{M}_2(t)\\ \bar{M}(t) + \tilde{M}_3(t)\end{bmatrix}, \tag{1}$$

where $\tilde{\theta}_i^{\mathrm{c}}(t)$, for $i \in \{1,2,3\}$, represent the perturbations in blade pitch demand from collective pitch angle signal $\bar{\theta}^{\mathrm{c}}(t)$. Similarly, $\tilde{M}_i(t)$, for $i \in \{1,2,3\}$, are the perturbations in flap-wise blade root bending moments, obtained by filtering out the average moment $\bar{M}(t)$ from the measurements $M_{1,2,3}(t)$. This structure is commonly used to separate the action of the IPC from that of the CPC (e.g. [1,2,24,25]). The relationship between collective pitch input $\bar{\theta}^{\mathrm{c}}$ and rotor speed output ω can be modelled by a transfer function $G_{\omega\theta} \in \mathcal{R}$ obtained by linearising the turbine dynamics around the operating conditions. In a similar fashion, the transfer function $G_{M\theta} \in \mathcal{R}$ relating each flap-wise blade bending moment output $\tilde{M}_i$ to additional pitch inputs $\tilde{\theta}_i^{\mathrm{c}}$ for $i \in \{1,2,3\}$ can also be found. For simplicity, it is assumed that there is no coupling between the CPC and IPC loops from the tower dynamics. These transfer functions are defined as follows:

$$G_{\omega\theta}(s) := G_{\mathrm{a}}(s)G_{\mathrm{r}}(s), \tag{2a}$$
$$G_{M\theta}(s) := G_{\mathrm{a}}(s)G_{\mathrm{b}}(s)G_{\mathrm{bp}}(s), \tag{2b}$$

where $G_{\mathrm{r}}, G_{\mathrm{b}}, G_{\mathrm{a}} \in \mathcal{R}$ describe the dynamics of rotor, blade and actuator, respectively, whilst $G_{\mathrm{bp}} \in \mathcal{R}$ is a band-pass filter that is included in order to remove the low and high frequency contents of the blade root bending moment

measurement signals, obtained from strain-gauge sensors. These transfer functions are defined as follows:

$$G_{\mathrm{r}}(s) := \frac{d\omega}{d\theta}\frac{1}{\tau_{\mathrm{r}}s+1}, \tag{3a}$$

$$G_{\mathrm{b}}(s) := \frac{dM_{\mathrm{flap}}}{d\theta}\frac{(2\pi f_{\mathrm{b}})^2}{s^2+4\pi f_{\mathrm{b}}D_{\mathrm{b}}s+(2\pi f_{\mathrm{b}})^2}, \tag{3b}$$

$$G_{\mathrm{a}}(s) := \frac{1}{\tau_{\mathrm{a}}s+1}, \tag{3c}$$

$$G_{\mathrm{bp}}(s) := \frac{2\pi f_{\mathrm{h}}s}{s^2+2\pi(f_{\mathrm{h}}+f_{\mathrm{l}})s+4\pi^2 f_{\mathrm{h}}f_{\mathrm{l}}}, \tag{3d}$$

where $\frac{d\omega}{d\theta}, \tau_{\mathrm{r}} \in \mathbb{R}$ denote the variation of aerodynamic torque to pitch angle and the time constant of the rotor dynamics, respectively, whilst $\frac{dM_{\mathrm{flap}}}{d\theta}$, $D_{\mathrm{b}}, f_{\mathrm{b}} \in \mathbb{R}$ represent the variation of flap-wise blade root bending moment to pitch angle, blade damping ratio and natural frequency of first blade mode, respectively. $\tau_{\mathrm{a}} \in \mathbb{R}$ denotes the time constant of the pitch actuator whilst $f_{\mathrm{h}}, f_{\mathrm{l}} \in \mathbb{R}$ represent the upper and lower cut-off frequencies of the band-pass filter, respectively. The values of those parameters are listed in Table III in Appendix A. The dynamics of rotor speed (3a) and pitch actuator (3c) are approximated as first-order systems respectively whilst the blade dynamics (3b) and band-pass filter (3d) are modelled as second-order systems. Note that the high-fidelity wind turbine employed for simulation purposes in this study operates across above-rated wind conditions and the parameters $\frac{d\omega}{d\theta}$ and $\frac{dM_{\mathrm{flap}}}{d\theta}$ vary based on operating wind conditions. For the linear models (3), a fixed set of parameters were obtained from linearisation of the simulation turbine model operating at $18\ \mathrm{ms}^{-1}$, chosen since this value is close to the centre of the range of wind speeds covering above-rated wind conditions.

2.2. Disturbance modelling

The rotor and blade are subjected to a temporally varying and spatially distributed wind field and in many studies, the feed-forward control assumes only a few points of wind measurement across the rotor disk to estimate the effective wind speed at the rotor and blade. Given the fact that the blade and rotor loads vary along the span of the blades, owing to the wind conditions and blade geometry, more wind measurements across the entire rotor plane will inevitably provide improved estimation of such loads. A number of studies demonstrated the feasibility of estimating the wind-field from a few point measurements taken upstream of the turbine (e.g. [26, 27]). Since this is a non-trivial problem, the issue of wind-field estimation is not considered in the present work. Instead, this work assumes the approaching stream-wise wind speeds are known apriori perfectly, and the focus of this work is to design a control algorithm that utilises such preview information.

The disturbance trajectories of rotor speed ω_d, and flap-wise blade bending moment $\tilde{M}_{d_i}$, for $i \in \{1,2,3\}$, caused by the approaching wind at sample time k, are defined as follows:

$$\omega_d(k) := \sum_{l,\phi}\frac{d\omega}{dv}(\bar{v},l)v(l,\phi,k), \tag{4a}$$

$$\tilde{M}_{d_i}(k) := \sum_{l,\phi}\frac{dM_{\mathrm{flap}}}{dv}(\bar{v},l)v(l,\phi,k), \tag{4b}$$

where $v(l,\phi,k) \in \mathbb{R}$ denote the stream-wise wind speed measurements where $l, \phi \in \mathbb{R}$ represent the radial and angular co-ordinates across the rotor disk whilst $\bar{v} \in \mathbb{R}$ denote the averaged wind speed of the measurements. The variations in rotor speed and blade bending moment with respect to the wind are denoted as $\frac{d\omega_d}{dv}$, $\frac{dM_d}{dv} \in \mathbb{R}$. The rotor speed response ω to wind-induced disturbance ω_d is modelled as a first-order transfer function $G_{\omega\omega_d} \in \mathcal{R}$, whilst the response of flap-wise blade root bending moment $\tilde{M}_i$ to wind-induced disturbance $\tilde{M}_{d_i}$, for $i \in \{1,2,3\}$, is modelled as $G_{MM_d} \in \mathcal{R}$:

$$G_{\omega\omega_d}(s) := \frac{1}{\tau_{\mathrm{r}}s+1}, \tag{5a}$$

$$G_{MM_d}(s) := \frac{(2\pi f_{\mathrm{b}})^2}{s^2+4\pi f_{\mathrm{b}}D_{\mathrm{b}}s+(2\pi f_{\mathrm{b}})^2}G_{\mathrm{bp}}(s), \tag{5b}$$

DOI: 10.1002/we
Prepared using weauth.cls

where the parameters are listed in Table III. Combining (2) and (5), the overall transfer function models $G \in \mathcal{R}^{4\times4}$ and $G_d \in \mathcal{R}^{4\times4}$ can be represented as follows:

$$\begin{bmatrix} \omega(s) \\ \tilde{M}_1(s) \\ \tilde{M}_2(s) \\ \tilde{M}_3(s) \end{bmatrix} = \underbrace{\begin{bmatrix} G_{\omega\theta}(s) & 0 & 0 & 0 \\ 0 & G_{M\theta}(s) & 0 & 0 \\ 0 & 0 & G_{M\theta}(s) & 0 \\ 0 & 0 & 0 & G_{M\theta}(s) \end{bmatrix}}_{G(s)} \begin{bmatrix} \bar{\theta}^{\mathrm{c}}(s) \\ \tilde{\theta}^{\mathrm{c}}_1(s) \\ \tilde{\theta}^{\mathrm{c}}_2(s) \\ \tilde{\theta}^{\mathrm{c}}_3(s) \end{bmatrix} + \underbrace{\begin{bmatrix} G_{\omega\omega_d}(s) & 0 & 0 & 0 \\ 0 & G_{MM_d}(s) & 0 & 0 \\ 0 & 0 & G_{MM_d}(s) & 0 \\ 0 & 0 & 0 & G_{MM_d}(s) \end{bmatrix}}_{G_d(s)} \begin{bmatrix} \omega_d(s) \\ \tilde{M}_{d_1}(s) \\ \tilde{M}_{d_2}(s) \\ \tilde{M}_{d_3}(s) \end{bmatrix}. \tag{6}$$

Equivalently, the model can be described in a discrete-time state-space form since the discrete-time model is more convenient in the MPC framework:

$$\begin{aligned} x_{\mathrm{p}}(k+1) &= A_{\mathrm{p}}x_{\mathrm{p}}(k) + B_{\mathrm{p}}u(k) + B_{\mathrm{d_p}}d(k), \\ y(k) &= C_{\mathrm{p}}x_{\mathrm{p}}(k), \end{aligned} \tag{7a}$$

where

$$u(k) = [\bar{\theta}^{\mathrm{c}}(k), \tilde{\theta}^{\mathrm{c}}_1(k), \tilde{\theta}^{\mathrm{c}}_2(k), \tilde{\theta}^{\mathrm{c}}_3(k)]^T, \tag{7b}$$

$$y(k) = [\omega(k), \tilde{M}_1(k), \tilde{M}_2(k), \tilde{M}_3(k)]^T, \tag{7c}$$

$$d(k) = [\omega_d(k), \tilde{M}_{d_1}(k), \tilde{M}_{d_2}(k), \tilde{M}_{d_3}(k)]^T, \tag{7d}$$

and the state vector $x_{\mathrm{p}} \in \mathbb{R}^{n_{x_{\mathrm{p}}}}$ of the model is a collection of variables that characterises the dynamics of the transfer functions G and G_d that map the input vector $u \in \mathbb{R}^{n_u}$ and disturbance vector $d \in \mathbb{R}^{n_d}$ into the output vector $y \in \mathbb{R}^{n_y}$. The subscript p denotes the plant.

2.3. Nominal robust feedback controller

The focus of this work is to design the MPC layer algorithm on top of a nominal output-feedback controller. The chosen feedback controller $K \in \mathcal{R}^{4\times4}$, consisting of CPC $K_{\theta\omega} \in \mathcal{R}$ and IPC $K_{\theta M} \in \mathcal{R}$ is defined as follows:

$$\begin{bmatrix} \bar{\theta}^{\mathrm{c}}(s) \\ \tilde{\theta}^{\mathrm{c}}_1(s) \\ \tilde{\theta}^{\mathrm{c}}_2(s) \\ \tilde{\theta}^{\mathrm{c}}_3(s) \end{bmatrix} = \underbrace{\begin{bmatrix} K_{\theta\omega}(s) & 0 & 0 & 0 \\ 0 & K_{\theta M}(s) & 0 & 0 \\ 0 & 0 & K_{\theta M}(s) & 0 \\ 0 & 0 & 0 & K_{\theta M}(s) \end{bmatrix}}_{K(s)} \begin{bmatrix} \omega(s) \\ \tilde{M}_1(s) \\ \tilde{M}_2(s) \\ \tilde{M}_3(s) \end{bmatrix}, \tag{8}$$

where $K_{\theta\omega}, K_{\theta M} \in \mathcal{R}$ are stabilising controllers for the system model G in (6) and these controllers are listed in Appendix A. With respect to $K_{\theta M}$, a variety of IPC strategies exists in the literature, for example, Coleman transform-based control [24, 25], Clarke transform-based control [28] and single-blade control [3]. The transform-based IPC techniques involve coordinate mappings on the pitch inputs which complicate the constraint formulation in MPC, where the constraint inequalities need to be updated on-line at every sample, based on the prediction of azimuth angle. In addition, as proved in [29], the performance differences between the various types of IPCs are negligible. Consequently, single-blade control IPC is employed in this work, where each blade is equipped with its own controller ($K_{\theta M}$) in response to a local blade load measurement. The diagonal structure of the controller (8) mirrors that of the plant model (6). Implicit in this structure is an assumption of no dynamic coupling between the fixed and rotating turbine structures. The simulation results in [29] showed that a controller of the form (8) could be designed to be insensitive to such coupling by shaping the open-loop frequency response to have low gain at the tower frequency. Similar to the plant model, the feedback controller (8) has a discrete-time state-space realisation:

$$\begin{aligned} x_\kappa(k+1) &= A_\kappa x_\kappa(k) - B_\kappa y(k), \\ u(k) &= C_\kappa x_\kappa(k) - D_\kappa y(k), \end{aligned} \tag{9}$$

where the state vector $x_\kappa \in \mathbb{R}^{n_{x_\kappa}}$ is a collection of variables that characterises the dynamics of the controller K and the subscript κ denotes controller.

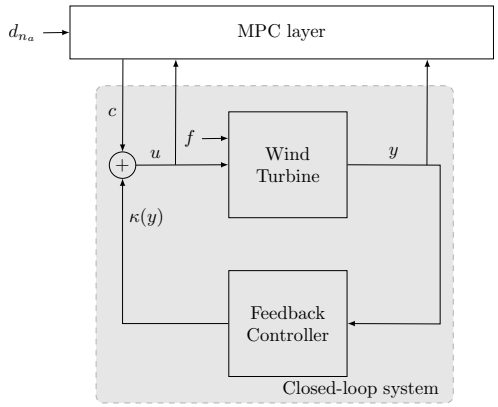

Figure 2. Schematic of model predictive control layer on top of an existing output-feedback controller.

3. DESIGN OF THE MODEL PREDICTIVE CONTROL LAYER

This section describes the design of the MPC layer to compliment the output-feedback blade-pitch controller (8) derived in the previous section. The architecture combining the predictive control layer and the separate feedback controller is shown in Figure 2, where the shaded area depicts the existing closed-loop system. A constrained optimisation based on the closed-loop system model predictions, which are dependent upon the plant output y, feedback action $\kappa(y)$ and upcoming disturbance measurement $\underset{\rightarrow}{d}$, is computed by the MPC layer at every sample and the optimal solution will be added into the closed-loop system, denoted as perturbation c in Figure 2. The closed-loop system model employed by the MPC layer will be discussed in the subsequent section.

3.1. State-space representation of the closed-loop system model

The closed-loop dynamic system model employed in the proposed MPC algorithm can be described by combining the linear wind turbine model (7) and controller (9), and the model is defined as follows:

$$\begin{bmatrix} x_{\mathrm{p}k+1} \\ x_{\kappa k+1} \end{bmatrix} = \underbrace{\begin{bmatrix} A_{\mathrm{p}} & 0 \\ -B_\kappa C_{\mathrm{p}} & A_\kappa \end{bmatrix}}_{A} \underbrace{\begin{bmatrix} x_{\mathrm{p}k} \\ x_{\kappa k} \end{bmatrix}}_{x_k} + \underbrace{\begin{bmatrix} B_{\mathrm{p}} \\ 0 \end{bmatrix}}_{B} u_k + \underbrace{\begin{bmatrix} B_{\mathrm{d_p}} \\ 0 \end{bmatrix}}_{B_{\mathrm{d}}} d_k, \tag{10a}$$

$$u_k = \begin{bmatrix} -D_\kappa C_{\mathrm{p}} & C_\kappa \end{bmatrix} x_k = K x_k, \tag{10b}$$

$$y_k = \begin{bmatrix} C_{\mathrm{p}} & 0 \end{bmatrix} x_k = C x_k. \tag{10c}$$

Notice that the (A, B) and (A, C) in this work are stabilizable and detectable, respectively. The states of the turbine model $x_{\mathrm{p}k} \in \mathbb{R}^{n_{x_{\mathrm{p}}}}$ cannot be measured directly and the separate nature of the feedback controller prohibits direct access to the states of the controller $x_{\kappa k} \in \mathbb{R}^{n_{x_\kappa}}$, thus, observers employed to estimate these states are described by the following expressions:

$$\hat{x}_{\mathrm{p}k+1|k} = A_{\mathrm{p}} \hat{x}_{\mathrm{p}k|k-1} + B_{\mathrm{p}} u_k + B_{\mathrm{d_p}} d_k + L_{\mathrm{p}}(y_k - \hat{y}_{k|k-1}), \quad \hat{y}_{k|k-1} = C_{\mathrm{p}} \hat{x}_{\mathrm{p}k|k-1}, \tag{11a}$$

$$\hat{x}_{\kappa k+1|k} = A_\kappa \hat{x}_{\kappa k|k-1} - B_\kappa y_k + L_\kappa(u_k - \hat{u}_{k|k-1}), \quad \hat{u}_{k|k-1} = C_\kappa \hat{x}_{\kappa k|k-1} - D_\kappa y_k, \tag{11b}$$

where $\hat{x}_{\mathrm{p}} \in \mathbb{R}^{n_{x_{\mathrm{p}}}}$ and $\hat{x}_\kappa \in \mathbb{R}^{n_{x_\kappa}}$ denote the estimates of the state of wind turbine model and controller, respectively, and $L_{\mathrm{p}} \in \mathbb{R}^{n_{x_{\mathrm{p}}} \times n_y}$ and $L_\kappa \in \mathbb{R}^{n_{x_\kappa} \times n_u}$ are the observer gains. It is noted that due to the mismatch between the wind turbine linear model and the high-fidelity turbine model, a difference exists between $y \in \mathbb{R}^{n_y}$ and $\hat{y} \in \mathbb{R}^{n_y}$, whilst in contrast, $\hat{u} \in \mathbb{R}^{n_u}$ converges to $u \in \mathbb{R}^{n_u}$ assuming no noise on the inputs.

3.2. Augmentation of the perturbations into the underlying feedback control law

This section describes the formulations of the predictions of state, input and disturbance with the degrees-of-freedom that are optimised by the MPC algorithm. The MPC layer formulation in this work adopts a dual-mode closed-loop paradigm (e.g. [30, 31]), whereby the perturbation $c_k \in \mathbb{R}^{n_u}$ is defined around a stabilising feedback control law $u_k = K x_k$ such that the input can be parametrised as $u_k = K x_k + c_k$. The premise behind this approach is that the MPC perturbation $c_k \neq 0$ if and only if constraints are active or feed-forward knowledge is available. Such a feature is particularly useful

DOI: 10.1002/we
Prepared using weauth.cls

in formulating an MPC layer on top of an embedded closed-loop controller. Notice that the perturbation sequence $\underset{\rightarrow k}{c} = [c_{0|k}, c_{1|k}, ..., c_{n_c-1|k}]^T \in \mathbb{R}^{n_u n_c}$ is optimised over the control horizon n_c, whist beyond n_c, the closed-loop dynamics are governed by the existing feedback pitch controller. Considering (10), the predictions of input and state can be described as follows:

$$u_{i|k} = \begin{cases} Kx_{i|k} + c_{i|k}, & \forall i < n_c, \\ Kx_{i|k}, & \forall i \geq n_c, \end{cases} \tag{12a}$$

$$x_{i+1|k} = \begin{cases} \Phi x_{i|k} + Bc_{i|k} + B_{\mathrm{d}} d_{i|k}, & \forall i < n_c, \\ \Phi x_{i|k} + B_{\mathrm{d}} d_{i|k}, & \forall i \geq n_c, \end{cases} \tag{12b}$$

where $\Phi = A + BK$ is strictly Hurwitz, whilst $u_{i|k} \in \mathbb{R}^{n_u}$ and $x_{i|k} \in \mathbb{R}^{n_x}$ denote, respectively, the predicted values of the model input and state at sample $k+i$ based on the measurement available at sample k. Note that $x_{0|k} = x_k$. The disturbance prediction sequence $\underset{\rightarrow k}{d} = [d_{0|k}, d_{1|k}, ..., d_{n_a-1|k}]^T \in \mathbb{R}^{n_d n_a}$ is defined as follows:

$$d_{i|k} = \begin{cases} d_{k+i}, & \forall i < n_a, \\ 0, & \forall i \geq n_a. \end{cases} \tag{12c}$$

The upcoming disturbance measurements are assumed to be zero beyond the preview horizon n_a. The predictions of states(12b), perturbations (12a) and disturbance (12c) can be expressed in a more convenient and compact autonomous form, where its state $z_{i|k} \in \mathbb{R}^{n_z}$ consists of the state $x_{i|k}$, perturbations $\underset{\rightarrow k}{c}$ and disturbance $\underset{\rightarrow k}{d}$, defined as follows:

$$z_{i+1|k} = \Psi z_{i|k}, \tag{13a}$$

where the initial state $z_{0|k} = [x_{0|k}, \underset{\rightarrow k}{c}, \underset{\rightarrow k}{d}]^T \in \mathbb{R}^{n_z}$ and Ψ is defined as:

$$\Psi = \begin{bmatrix} \Phi & BE & B_d E \\ 0 & M_c & 0 \\ 0 & 0 & M_d \end{bmatrix}, \tag{13b}$$

$$E \underset{\rightarrow k}{c} = c_{0|k}, \quad E \underset{\rightarrow k}{d} = d_{0|k}, \tag{13c}$$

$$M_c \underset{\rightarrow k}{c} = [c_{1|k}, \ldots, c_{n_c-1|k}, 0]^T, \tag{13d}$$

$$M_d \underset{\rightarrow k}{d} = [d_{1|k}, \ldots, d_{n_a-1|k}, 0]^T, \tag{13e}$$

where the details of the matrices $M_c \in \mathbb{R}^{n_u n_c \times n_u n_c}$, $M_d \in \mathbb{R}^{n_d n_a \times n_d n_a}$ and $E \in \mathbb{R}^{n_x \times n_u n_c}$ are provided in Appendix B. Consequently, the predictions of inputs (12a) and states (12b) can be expressed in terms of the autonomous form as follows:

$$u_{i|k} = \begin{bmatrix} K & E & 0 \end{bmatrix} z_{i|k}, \quad \forall i \geq 0, \tag{14a}$$

$$x_{i|k} = \begin{bmatrix} I & 0 & 0 \end{bmatrix} z_{i|k}, \quad \forall i \geq 0. \tag{14b}$$

This autonomous form of predictions (14) will be used in conjunction with a cost function to compute the perturbation sequence $\underset{\rightarrow k}{c}$ in the following section.

3.3. Formulation of the cost function

The perturbation sequence $\underset{\rightarrow k}{c}$ can be computed by solving a constrained minimisation of the predicted cost on-line where the predicted cost function quantifying the balance between performance and input effort is defined as follows:

$$J := \sum_{i=0}^{\infty} x_{i|k}^T Q x_{i|k} + u_{i|k}^T R u_{i|k}, \tag{15a}$$

where $Q \in \mathbb{R}^{n_x \times n_x}$ and $R \in \mathbb{R}^{n_u \times n_u}$ denote the weights that specify the penalties on state and input, respectively. For practical reasons, the infinite-horizon cost index (15a) needs to be compacted into a finite-horizon form such that the cost function can be solved on-line rapidly using quadratic programming. By expressing the predictions of the state and input into the autonomous form as (14b) and (14a), the infinite-horizon cost function (15a) can be simplified as follows:

$$J = \sum_{i=0}^{\infty} z_{i|k}^T (\Gamma_x^T Q \Gamma_x + \Gamma_u^T R \Gamma_u) z_{i|k}, \tag{15b}$$

where $\Gamma_x = \begin{bmatrix} I & 0 & 0 \end{bmatrix} \in \mathbb{R}^{n_x \times n_z}$ and $\Gamma_u = \begin{bmatrix} K & E & 0 \end{bmatrix} \in \mathbb{R}^{n_u \times n_z}$. Consequently, the cost function (15b) can be further simplified, using the Lyapunov equation $\Psi^T S \Psi = S - W$ and $z_{i|k} = \Psi^i z_{0|k}$, as:

$$\begin{aligned} J &= z_{0|k}^T \underbrace{\sum_{i=0}^{\infty} \left({\Psi^i}^T \underbrace{\Gamma_x^T Q \Gamma_x + \Gamma_u^T R \Gamma_u}_{W} \Psi^i \right)}_{S} z_{0|k} \\ &= \begin{bmatrix} x_{0|k} \\ \underset{\rightarrow k}{c} \\ \underset{\rightarrow k}{d} \end{bmatrix}^T S \begin{bmatrix} x_{0|k} \\ \underset{\rightarrow k}{c} \\ \underset{\rightarrow k}{d} \end{bmatrix} = \begin{bmatrix} x_{0|k} \\ \underset{\rightarrow k}{c} \\ \underset{\rightarrow k}{d} \end{bmatrix}^T \begin{bmatrix} S_x & S_{xc} & S_{xd} \\ S_{xc}^T & S_c & S_{cd} \\ S_{xd}^T & S_{cd}^T & S_d \end{bmatrix} \begin{bmatrix} x_{0|k} \\ \underset{\rightarrow k}{c} \\ \underset{\rightarrow k}{d} \end{bmatrix}, \\ &= \underset{\rightarrow k}{c}^T S_c \underset{\rightarrow k}{c} + 2 \underset{\rightarrow k}{c}^T S_{xc}^T x_{0|k} + 2 \underset{\rightarrow k}{c}^T S_{cd} \underset{\rightarrow k}{d} + \epsilon, \end{aligned} \tag{15c}$$

where ϵ denotes the terms that are independent of $\underset{\rightarrow}{c}$ and $x_{0|k} = x_k$. To complete the formulation of the constrained minimisation, the following section will demonstrate how to construct the constraint linear inequalities in terms of the perturbation sequence $\underset{\rightarrow k}{c}$.

3.4. Constraint formulation in terms of the perturbations

The constraints considered in this work are the angles and rates of the blade-pitch actuators and the rotor speed as follows:

$$\theta_{\min} - \varepsilon_{i|k}^{\theta} \leq \theta_{i|k} \leq \theta_{\max} + \varepsilon_{i|k}^{\theta}, \qquad \forall i \geq 0, \tag{16a}$$

$$\dot{\theta}_{\min} - \varepsilon_{i|k}^{\dot{\theta}} \leq \dot{\theta}_{i|k} \leq \dot{\theta}_{\max} + \varepsilon_{i|k}^{\dot{\theta}}, \qquad \forall i \geq 0, \tag{16b}$$

$$\omega_{i|k} \leq \omega_{\max} + \varepsilon_{i|k}^{\omega}, \qquad \forall i \geq 0, \tag{16c}$$

where $\theta = [\theta_1, \theta_2, \theta_3]^T \in \mathbb{R}^3$, whereas $\theta_{\min}, \theta_{\max}, \dot{\theta}_{\min}, \dot{\theta}_{\max} \in \mathbb{R}^3$ denote the minimum and maximum of the angle and rate of the pitch actuators, respectively, whilst $\omega_{\max} \in \mathbb{R}$ represents the maximum rotor speed. Since the constraints on pitch actuators and rotor speed are state-constraints, thus, the slack variables $\varepsilon_{i|k} = [\varepsilon_{i|k}^{\theta}, \varepsilon_{i|k}^{\dot{\theta}}, \varepsilon_{i|k}^{\omega}]^T \geq 0 \in \mathbb{R}^{n_\varepsilon}$ were employed to soften the constraints to ensure the feasibility of the optimisation if necessary. To minimise the predictions of the slack variables $\underset{\rightarrow k}{\varepsilon} = [\varepsilon_{0|k}, ..., \varepsilon_{n_c-1|k}]^T \in \mathbb{R}^{n_\varepsilon n_c}$, a quadratic penalty together with l_1-norm penalty is added into the cost (15c), as follows:

$$J = \underset{\rightarrow k}{c}^T S_c \underset{\rightarrow k}{c} + 2 \underset{\rightarrow k}{c}^T S_{xc}^T x_{0|k} + 2 \underset{\rightarrow k}{c}^T S_{cd} \underset{\rightarrow k}{d} + \underset{\rightarrow k}{\varepsilon}^T S_\varepsilon \underset{\rightarrow k}{\varepsilon} + L_\varepsilon^T \underset{\rightarrow k}{\varepsilon}. \tag{17}$$

The weights of the quadratic penalty $S_\varepsilon \in \mathbb{R}^{n_\varepsilon n_c \times n_\varepsilon n_c}$, that is a diagonal matrix, penalises the peak of constraint violations, whilst the weights of the l_1-norm penalty $L_\varepsilon \in \mathbb{R}^{n_\varepsilon n_c}$ penalises the total sum of violations [32]. Details of tunings are provided in Section 5.1.3.

Subsequently, the inequalities (16) can be written in terms of the autonomous form (13), with $z_{i|k} = \Psi^i z_{0|k}$, as follows:

$$H \Psi^i z_{0|k} \leq h + h_{i|k}^{\varepsilon}, \quad \forall i \geq 0, \tag{18}$$

where the matrices are chosen as $H z_{i|k} = [\theta_{i|k}, -\theta_{i|k}, \dot{\theta}_{i|k}, -\dot{\theta}_{i|k}, \omega_{i|k}]^T, h = [\theta_{\max}, -\theta_{\min}, \dot{\theta}_{\max}, -\dot{\theta}_{\min}, \omega_{\max}]^T$ and $h_{i|k}^{\varepsilon} = [\varepsilon_{i|k}^{\theta}, -\varepsilon_{i|k}^{\theta}, \varepsilon_{i|k}^{\dot{\theta}}, -\varepsilon_{i|k}^{\dot{\theta}}, \varepsilon_{i|k}^{\omega}]^T$. Notice that to ensure no constraint violations, possible violations in (18) must be checked over an infinite prediction horizon, which would appear to be computationally impractical. However, it is well known [33] that there exists a sufficiently large horizon where any additional linear equalities of (18) for $i \geq n_\infty$ become redundant, since Φ is strictly Hurwitz, $c_{i|k} = 0$ for $i \geq n_c$ and $d_{i|k} = 0$ for $i \geq n_a$. Consequently, for a practical approach, to compromise between the computational speed and constraint satisfaction, this study formulates the inequalities by checking the constraints over twice the control horizon. The inequalities can be described by a set of suitable matrices ($\mathcal{M}, \mathcal{N}, \mathcal{V}, \mathcal{T}$ and b) as follows:

$$\mathcal{M} x_{0|k} + \mathcal{N} \underset{\rightarrow k}{c} + \mathcal{V} \underset{\rightarrow k}{d} - \mathcal{T} \underset{\rightarrow k}{\varepsilon} \leq b, \tag{19}$$

The matrices $\mathcal{M}, \mathcal{N}, \mathcal{V}, \mathcal{T}$ and b can be computed off-line and hence only the variables $x_{0|k}$, $\underset{\rightarrow k}{c}$, $\underset{\rightarrow k}{d}$ and $\underset{\rightarrow k}{\varepsilon}$ need to be updated on-line.

To sum up Section 3, the proposed MPC layer, at each sample k, employs the states $x_k = x_{0|k}$ of the closed-loop system and subsequently determines the optimal perturbation sequence $\underset{\rightarrow k}{c}$ that takes into account both upcoming measurements and constraints, by solving a constrained minimisation of the predicted cost (17) subject to constraints (19). This is summarised in Algorithm 1.

DOI: 10.1002/we
Prepared using weauth.cls

Algorithm 1
At each sampling instant perform the constrained optimisation below. The first block element $c_k = c_{0|k}$ of the perturbation sequence is applied within the embedded control law, where $u_k = Kx_k + c_k$:

$$\min_{\underset{\rightarrow k}{c}, \underset{\rightarrow k}{\varepsilon}} \underset{\rightarrow k}{c}^T S_c \underset{\rightarrow k}{c} + 2\underset{\rightarrow k}{c}^T (S_{cd} \underset{\rightarrow k}{d} + S_{xc}^T x_{0|k}) + \underset{\rightarrow k}{\varepsilon}^T S_\varepsilon \underset{\rightarrow k}{\varepsilon} + L_\varepsilon^T \underset{\rightarrow k}{\varepsilon}, \tag{20a}$$

$$\text{s.t.} \quad \mathcal{M} x_{0|k} + \mathcal{N} \underset{\rightarrow k}{c} + \mathcal{V} \underset{\rightarrow k}{d} - \mathcal{T} \underset{\rightarrow k}{\varepsilon} \leq b. \tag{20b}$$

4. ANALYSIS OF THE PREDICTIVE CONTROL LAYER DESIGN

In the following sections, we will investigate in what conditions the original feedback closed-loop dynamics remain unchanged by the additional control layer design.

4.1. A motivating example

The aim of this motivating example is to illustrate that the perturbations from the MPC layer could introduce an additional feedback loop into the given closed-loop system. The original feedback control input is given by (10b) as follows:

$$u_k = Kx_k. \tag{21a}$$

The additional perturbation c_k computed from the control layer will be added into (21a), thus, the new control law becomes:

$$u_k = Kx_k + c_k. \tag{21b}$$

Considering an unconstrained minimisation of the cost function in Algorithm 1, the perturbation c_k is as follows:

$$c_k = E \underset{\rightarrow k}{c} = -\underbrace{E S_c^{-1} S_{xc}^T}_{K_c} x_{0|k} - \underbrace{E S_c^{-1} S_{cd}}_{P_d} \underset{\rightarrow k}{d}, \tag{22}$$

where $x_{0|k} = x_k$. Consequently, substituting (22) into (21b), the new control law becomes:

$$u_k = (K - K_c)x_k - P_d \underset{\rightarrow k}{d}. \tag{23}$$

Compared to the original control input (21a), the feedback gain of the new control law (23) is altered by the additional feedback loop introduced by the control layer design, thus, the original closed-loop dynamics are not preserved. This mixed nature of control layer design has several disadvantages:

1. The performance and robustness properties of the nominal feedback controller are no longer guaranteed to be retained. In practice, existing blade-pitch feedback controllers are carefully tuned so as not to excite tower dynamics, and so any additional control law that interfered in this could be disastrous.
2. Tuning of the additional control layer becomes difficult since the perturbation c_k from the mixed structure introduces an additional feedback loop that needs to satisfy the robustness concerns.
3. The performance benefit from using real-time measurement of the approaching wind field can not be clearly distinguished from the feedback control because of the additional feedback loop from the extra control layer.

Thus, in the next section, we will investigate the conditions that enables the separate structure design where the additional control layer provides solely the feed-forward input and constraint handling capability, with the dynamics of the nominal closed-loop system remaining unaffected whilst constraints are not violated.

4.2. Conditions for separating the original closed-loop dynamics from the additional layer design

Close inspection of the unconstrained optimal perturbation sequence (22) suggests that, to retain the closed-loop robust properties, the perturbation sequence c_k must be independent of the state $x_{0|k}$ (i.e. S_{xc}^T = 0 in the cost). Thus, the key result of this paper is as follows:

Theorem 1
The unconstrained perturbation sequence $\underset{\rightarrow}{c}$ from the additional control layer (Algorithm 1) has no impact on the original closed-loop dynamics if and only if $S_{xc}^T = 0$. For $S_{xc}^T = 0$, the cost function in Algorithm 1 needs to embed some knowledge of the nominal output-feedback control law (10b) such that the weights Q, R and S_x satisfy the following conditions:

$$\Phi^T S_x \Phi - S_x + Q + K^T R K = 0, \tag{24a}$$

$$B^T S_x \Phi + RK = 0. \tag{24b}$$

Proof
See Appendix C. □

Corollary 1
Theorem 1 demonstrates that the extra control layer that satisfies the conditions (24) will not impact on the underlying robust output-feedback control law unless constraints are predicted to be active. Consequently, in normal operation, the properties of the original closed-loop dynamics are retained and the additional control layer solely handles the real-time upcoming wind information.

The underlying output-feedback controllers (9) employed in this work were designed using frequency-shaping techniques. Thus, with the pre-determined stabilising controller K, weights $Q > 0$ could be chosen and subsequently, the remaining weights S_x and R that satisfy (24) can be determined by solving a linear matrix inequality (LMI) problem [34].

For most of the time, the constraints employed in this work are not expected to be violated. Nevertheless, when constraints are active, the robustness of the feedback closed-loop dynamics cannot be retained as the perturbation c_k impacts the closed-loop and it becomes non-trivial to prove robust stability. The proof requires the constraints tightened by the possible uncertainties and solving an optimisation based on the tightened constraints might result in a conservative and computationally demanding control law [31]. In contrast, the proposed methods of designing the MPC layer upon a given robust feedback controller might offer an alternative and practical solution since the guarantee of constraint fulfilment is less crucial to the wind turbine blade-pitch problem. Furthermore, given that the closed-loop prediction structures employed in the MPC layer are robust to uncertainties, one would expect such robust properties are likely to carry over to cases where constraints are predicted to be active.

5. NUMERICAL RESULTS AND DISCUSSIONS

The aims of this section are to demonstrate the benefits gained by deploying the proposed MPC layer on top of the nominal robust feedback controller. The separate nature of the proposed design offers a transparent framework to distinguish the marginal improvement by deploying various features, for example, the capability of handling upcoming disturbance information or constraint violations, into the nominal controller. This provides insights for wind turbine manufacturers to evaluate the benefits against the associated cost of each feature. The results were obtained from closed-loop simulations upon a high-fidelity wind turbine.

5.1. Simulation environment and settings

In this section, the details of the turbine simulation are presented and also the estimation methods of the upcoming disturbance trajectories of the rotor speed and blade moments are discussed. Furthermore, it is followed by the selections of control and preview horizon and constraints for the MPC layer.

5.1.1. Simulation environment

The turbine model employed in this study is the NREL 5MW baseline turbine [35] based on the FAST code [36]. This model is of much greater complexity than the model (6) employed for control design and includes flap-wise and edge-wise blade modes, in addition to the tower and drive train dynamics. Also, a baseline generator torque controller [35] is employed in this study; in above-rated conditions the torque command is inversely proportional to the rotor speed with the purpose to prevent overloading the generator. Closed-loop simulations were performed under a set of representative and turbulent wind fields generated by the TurbSim code [37]. These full-field three-dimensional wind data were characterised by mean wind speeds, turbulence settings and wind shear exponent. The TurbSim code simulated a time series of wind data at points in a two-dimensional 17-by-17 grid such that the sequence of grids march towards the rotor at a constant speed specified by the mean wind speed and under the assumption of Taylor's frozen turbulence hypothesis.

5.1.2. Future measurements of rotor speed and blade disturbance

As discussed in Section 2.2, the issue of wind-field estimation is a non-trivial problem, this work assumes the disturbance trajectories of rotor speed and flap-wise blade bending moments are estimated based on the prefect stream-wise wind speed measurements in front of the turbine. To examine the accuracy of the estimated disturbance trajectories generated from (4), comparisons were made against the actual trajectories obtained from the non-linear turbine simulation, shown in Figure 3. The time series of the disturbance trajectories of rotor speed deviation $\Delta\omega$ and flap-wise bending moment of blade 1 $\tilde{M}_1$ are illustrated in Figure 3(a) and 3(b) and it reveals that the disturbance trajectories obtained from the linear model and non-linear turbine are almost identical. Figure 3(c) and 3(d) reveal the frequency spectra of the time series of both trajectories, which confirms that both trajectories are alike, as demonstrated by the similarity in the magnitudes at the dominant frequencies that is below 0.1 Hz for rotor speed and at 0.2 Hz for blade moment.

DOI: 10.1002/we
Prepared using weauth.cls

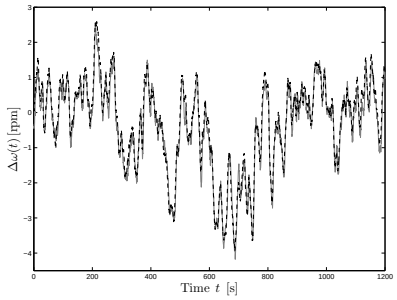

(a) Time series of the disturbance trajectories of rotor speed deviation.

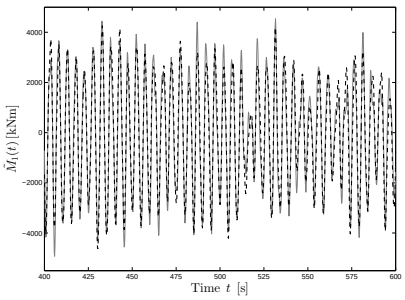

(b) Time series of the disturbance trajectories of flap-wise bending moment of blade 1.

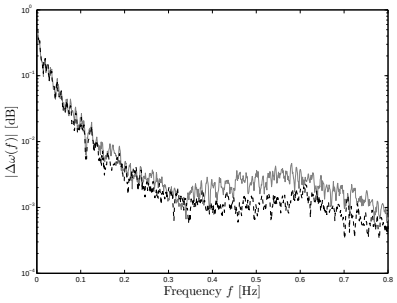

(c) Frequency spectrum of disturbance trajectories of rotor speed.

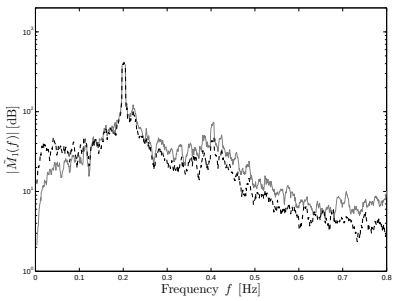

(d) Frequency spectrum of disturbance trajectories of blade bending moment.

Figure 3. Comparison between the disturbance trajectories obtained from the linear model (dash line) and non-linear turbine (solid line). Simulation data was obtained under a turbulent wind field characterised by the mean speed of 18 ms^{-1} and turbulence intensity of 14%. Similar results were observed for the remaining blades.

5.1.3. Choice of the MPC horizons, constraints and weights

The predictive controller should anticipate the upcoming disturbance far ahead enough to allow beneficial feed-forward compensation. A preview horizon of $n_a = 15$ samples was found a reasonable choice in the present simulation setting. The operating frequency of the MPC controller was 5 Hz which provided a satisfactory compromise between performance and computational burden; hence the preview horizon period was of duration three seconds. A similar idea also holds true for the control horizon n_c. The control horizon should be at least as large as the preview horizon, for the reason that the MPC controller can then plan an effective contemporaneous control sequences to compensate for the upcoming disturbance [38].

The pitch actuators employed in this study is bounded between 0 and 90 degrees and ± 8 degrees per second. In addition, constraint is also placed on the maximum rotor speed to avoid excessive loads on the generator, which is chosen as 0.725 rpm (6%) above the rated rotor speed.

Tuning of the weights of the MPC layer Q and R in the cost (15a) is intuitive, where such a choice rests largely with the preference for output performance compared to the control effort of the perturbation $\underset{\rightarrow}{c}$. In addition, the weights also need to satisfy the conditions (24) in Theorem 1.Ttuning of the weights of the quadratic penalty S_ε and l_1-norm penalty L_ε in the cost (17) is dependent on the trade-off between the duration and peak of the constraint violations. To illustrate, Figure 4 shows simulation results of constraint violations on the rotor speed deviation, where the diagonal entries of S_ε are $s_\varepsilon > 0 \in \mathbb{R}$ and the elements of L_ε are $l_\varepsilon > 0 \in \mathbb{R}$. It is clearly seen in Figure 4 that increasing the relative importance of the quadratic penalty s_ε compared to the l_1-norm penalty l_ε results in prolonging the duration of the constraint violation but a reduction in the peak violation. Given that over speeding the rotor beyond a certain threshold could potentially cause the turbine to trigger a temporary shut down, there is a good argument that it is more favourable to minimise the size of violation. Nonetheless, the l_ε need to be chosen large enough to ensure the soft constraint to be exact, which implies the slack variables are enforced to zero whenever a feasible solution of the optimisation is possible [32].

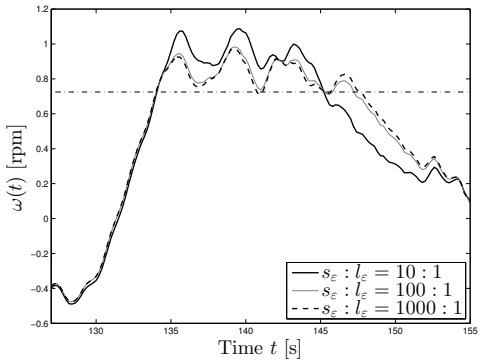

Figure 4. Soft constraint on rotor speed deviation with different quadratic and linear weights, s_ε and l_ε, respectively, on the slack variables. Dash-dot line denotes the maximal speed deviation of 0.725 rpm.

Controllers	Availability of of ω_d	Availability of $\tilde{M}_d$	Constraint handling
FB (baseline)			
FB/FF$_{\omega_d}$	✓		
FB/FF$_{\omega_d M_d}$	✓	✓	
FB/MPC$_{\omega_d}$	✓		✓
FB/MPC$_{\omega_d M_d}$	✓	✓	✓

Table I. Various control configurations employed in this study. With the nominal feedback controller as the baseline, additional features such as feed-forward knowledge and constraint handling are incrementally augmented into the feedback controller.

5.2. Simulation results

In section 5.2.1, time history samples were extracted from simulation results to investigate the performance gained by utilising upwind measurements of disturbance and constraint handling. This is followed by analysis of full results obtained from simulations under various wind conditions in Section 5.2.2.

5.2.1. Case studies: Benefits of utilising upcoming measurments and constraint handling

This section examines the improvement from deploying the MPC layer in cases when constraint violations are expected. Three controllers, detailed in Table I, were compared: (i) the baseline nominal feedback-only controller (9), denoted as FB; (ii) a preview controller that utilises the advance measurements of rotor speed and blade disturbance but no constraint handling capability, denoted as FB/FF$_{\omega_d M_d}$; and (iii) the final controller is a preview and constraint-aware controller and its control law obtained by solving Algorithm 1 on-line, denoted FB/MPC$_{\omega_d M_d}$. Three types of constraints were employed in this work, thus, comparisons were made for three classes of constraint violations.

Figure 5, 6 and 7 show, respectively, the performance comparisons in cases when the rotor speed, actuator pitch angle and rate constraints are expected. It can be clearly seen in Figure 5 that both controllers, FB/FF$_{\omega_d M_d}$ and FB/MPC$_{\omega_d M_d}$, outperform the baseline controller FB since they use advance measurements. Furthermore, the time history of rotor speed in Figure 5(a) indicates that the constraint-aware controller FB/MPC$_{\omega_d M_d}$ anticipated and avoided violating the maximum rotor speed constraint. Similar blade loads and pitch activities are observed in Figure 5(b), 5(c) and 5(d).

Figure 6 presents results where the blade pitch actuators steer near the lower limit. Owing to advance knowledge of the disturbance, it is not surprising that the preview controllers, FB/FF$_{\omega_d M_d}$ and FB/MPC$_{\omega_d M_d}$, perform better on rotor speed tracking and blade load reduction than the baseline controller FB as shown in 6(a) and 6(b). In addition, Figure 6(a) and 6(b) reveal that significant reductions in the rotor speed deviation and flap-wise blade bending moments were achieved by the controller FB/MPC$_{\omega_d M_d}$ which is aware of the actuator constraints, as evident in Figure 6(c).

The situation where the pitch actuators operate close to its maximum rate is illustrated in Figure 7. As shown in Figure 7(b), better reductions in the flap-wise blade bending moment were yielded by the constraint-aware preview controller, FB/MPC$_{\omega_d M_d}$, that foresees the pitch rate violations, as indicated in Figure 7(d). In general, it is apparent that constraint anticipations of pitch rates provide the least benefit contrary to pitch angle and rotor speed constraints. Nevertheless. this seems plausible because pitch actuators operate at the maximum rate for a relatively short period, typically less than one second. Thus, the controller that foresee the rate constraint might only achieve limited benefits given the fast blade dynamics.

DOI: 10.1002/we
Prepared using weauth.cls

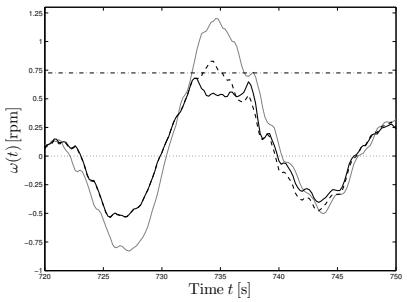

(a) Time history of the rotor speed deviation. Dash-dot line represents the constraint and dot line denotes the rated speed.

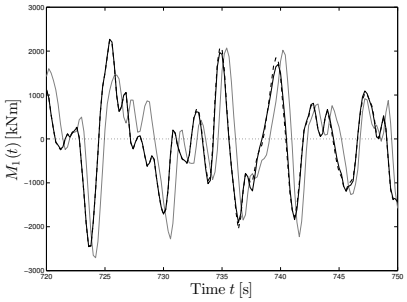

(b) Time history of the perturbations in flap-wise blade root bending moment of blade 1. Dot line denotes the performance target.

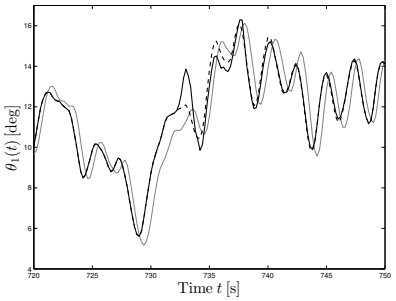

(c) Time history of the pitch angle of blade 1.

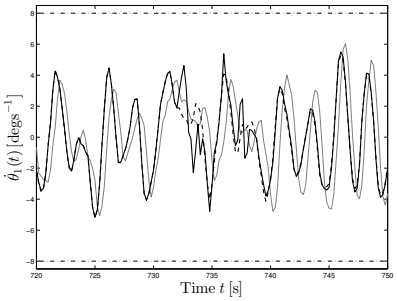

(d) Time history of the pitch rate of blade 1. Dash-dot lines represent the pitch rate constraints.

Figure 5. Simulation results upon the NREL 5MW turbine operating in a wind case with the mean speed of 19 ms^{-1} and turbulence intensity of 14%, showing the performance of the various controllers studied in this paper. Similar behaviours are obtained for the remaining blades. (i) Thin grey line: FB. (ii) Thick dash line: FB/FF$_{\omega_d M_d}$. (iii) Thick solid line: FB/MPC$_{\omega_d M_d}$.

5.2.2. Simulation results under various wind cases

This section presents results obtained from closed-loop simulations under numerous wind cases. These wind cases are characterised by a mean speed between $13\mathrm{ms}^{-1}$ and $23\mathrm{ms}^{-1}$, spanning a large range of above-rated wind conditions, and turbulence intensity ranging from 14% to 18%. Two more preview controllers, summarised in Table I, were considered: FB/FF$_{\omega_d}$ and FB/MPC$_{\omega_d}$ and such controllers are the same as FB/FF$_{\omega_d M_d}$ and FB/MPC$_{\omega_d M_d}$, respectively, except that the upcoming measurements of blade disturbance are not available. The performance box plots of the result data generated from 180 sets of 20-minute simulations are shown in Figure 8. Each box represents the first and third quartiles whilst the band within the box represents the median of the dataset. The whiskers denote 5% and 95% quantiles. The data beyond the whiskers are considered as outliers, indicated by dots.

Figure 8(a) presents the box plot of the rotor speed performance. It can be clearly seen that the preview controllers achieved better reductions in rotor speed deviation compared to the baseline feedback-only controller, owing to the upcoming measurements of rotor speed disturbance trajectories. Moreover, the constraint-aware controllers manage to retain the rotor speed within the limit for most of the time despite the fact that the constraints on rotor speed were occasionally relaxed to ensure feasibility of the constrained optimisation of the MPC layer. These results indicate that proper management of constraint violations can lead to significant reductions in rotor speed.

Referring to Figure 8(b), the box plot shows the blade flap-wise root bending moment. Performance achieved by the controllers without the upcoming measurements of blade loads M_d was almost identical. In contrast, better reductions in the flap-wise blade moments were yielded by both preview controllers with knowledge of future blade loads. Close inspection between these two controllers reveals that the constraint-aware controller FB/MPC$_{\omega_d M_d}$ performed slightly better than the preview-only controller FB/FF$_{\omega_d M_d}$, which is consistent with the previous findings in Section 5.2.1.

The pitch angle and pitch rate command of blade 1 are illustrated by box plots in Figure 8(c) and 8(d), respectively. Note that the pitch angle command θ_1^c and pitch rate command $\dot{\theta}_1^c$ are considered instead of the pitch actuator activities because such activities are almost identical for five controllers and investigation of pitch command signals reveals how constraints were handled by each controller. Results in Figure 8(c) and 8(d) are as expected, that the MPC-based controllers were well

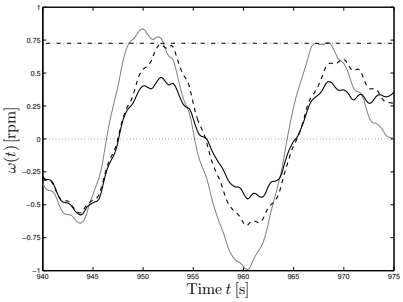

(a) Time history of the rotor speed deviation. Dash-dot line represents the constraint and dot line denotes the rated speed.

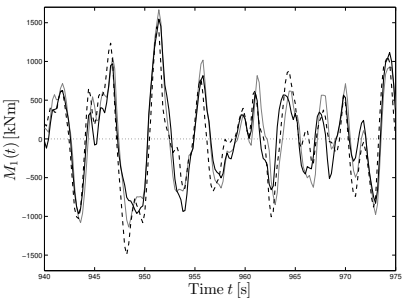

(b) Time history of the perturbations in flap-wise blade root bending moment of blade 1. Dot line denotes the performance target.

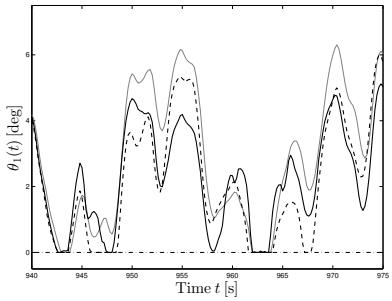

(c) Time history of the pitch angle of blade 1. Dash-dot line represents the lower pitch angle constraint.

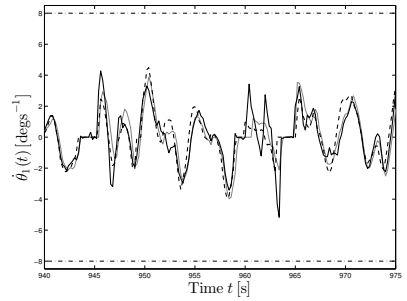

(d) Time history of the pitch rate of blade 1. Dash-dot lines represent the pitch rate constraints.

Figure 6. Simulation results upon the NREL 5MW turbine operating in a wind case with the mean speed of 13 ms^{-1} and turbulence intensity of 14%, showing the performance of the various controllers studied in this paper. Similar behaviours are obtained for the remaining blades. (i) Thin grey line: FB. (ii) Thick dash line: FB/FF$_{\omega_d M_d}$. (iii) Thick solid line: FB/MPC$_{\omega_d M_d}$.

	FB (Baseline)	FB/FF$_{\omega_d}$	FB/FF$_{\omega_d M_d}$	FB/MPC$_{\omega_d}$	FB/MPC$_{\omega_d M_d}$
std($\Delta\omega$) [rpm]	0.37 (100.00%)	0.22 (59.46%)	0.22 (59.46%)	0.21 (56.76%)	0.21 (56.76%)
std($\tilde{M}_1$) [MNm]	1.03 (100.00%)	1.01 (99.03%)	0.77 (74.76%)	1.01 (98.06%)	0.72 (69.90%)
std($\dot{\theta}_1$) [degs^{-1}]	2.53 (100.00%)	2.48 (98.02%)	2.50(98.81%)	2.58 (101.98%)	2.58 (101.98%)
max($\Delta\omega$) [rpm]	1.45 (100.00%)	1.05 (72.41%)	1.05 (72.41%)	0.76 (52.41%)	0.77 (53.10%)
max($\tilde{M}_1$) [MNm]	5.79 (100.00%)	5.70 (98.45%)	3.96 (67.36%)	5.70 (98.45%)	3.73 (64.42%)
Pr($\Delta\omega \geq \omega_{\max}$) [%]	2.15%	0.18%	0.20%	0.01%	0.01%
Pr($\theta_1^c \geq \pm\bar{\theta}_1$) [%]	0.55%	1.82%	1.82%	0.07%	0.07%
Pr($\dot{\theta}_1^c \geq \pm\dot{\theta}_1$) [%]	0.21%	0.22%	0.23%	0.10%	0.08%

Table II. Summary of simulation results upon the NREL 5MW turbine. Noted that std and max denote the standard deviation and maximum value, respectively. Pr represents the possibility of constraint violations. Differences in percentage to the baseline controller are represented in brackets.

aware of the constraints and managed most the commands to avoid operating beyond those constraints. Few outliers beyond the pitch angle and rate constraints can be observed in Figure 8(c) and 8(d).This is conceivable since soft constraints are imposed on those variables.

The results from this section are summarised in Table II. In general, the results suggested that controllers with more features performed better than those without them. Nevertheless, the cost and technical complexity associated with each layer are different, for example, in practice, the preview measurement of rotor disturbance could be estimated based on an averaged wind speed of few point measurements across the rotor disk whereas accurate estimations of the upcoming blade

Wind Energ. 2010; **00**:1–19 © 2010 John Wiley & Sons, Ltd.
DOI: 10.1002/we
Prepared using weauth.cls

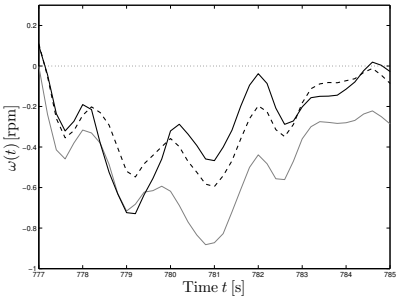

(a) Time history of the rotor speed deviation. Dot line denotes the rated speed.

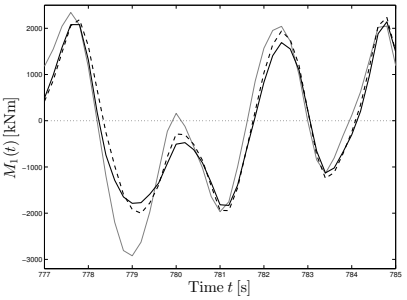

(b) Time history of the perturbations in flap-wise blade root bending moment of blade 1. Dot line denotes the performance target.

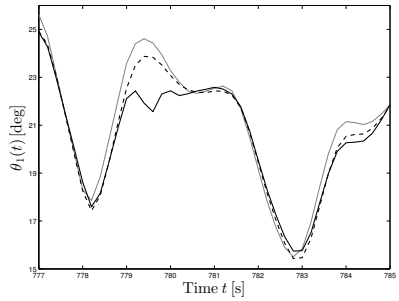

(c) Time history of the pitch angle of blade 1.

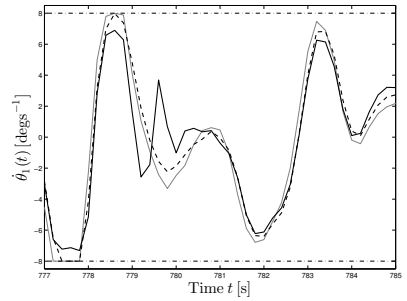

(d) Time history of the pitch rate of blade 1. Dash-dot lines represent the pitch rate constraints.

Figure 7. Simulation results upon the NREL 5MW turbine operating in a wind case with the mean speed of 23 ms^{-1} and turbulence intensity of 18%, showing the performance of the various controllers studied in this paper. Similar behaviours are obtained for the remaining blades. (i) Thin grey line: FB. (ii) Thick dash line: FB/FF$_{\omega_d M_d}$. (iii) Thick solid line: FB/MPC$_{\omega_d M_d}$.

disturbance are less trivial. As a whole, these results could be used as a representative guide on the potential performance benefits achievable by additional control features.

6. CONCLUSION

In this paper, the formulation of a modular predictive feed-forward layer on top of a robust output-feedback blade-pitch compensator is presented, together with the conditions to ensure the former does not interfere with the closed-loop dynamics provided by the latter. These conditions ensure that the additional predictive control layers only handles upcoming real-time measurements and impacts the closed-loop properties if and only if there are constraint violations. The separate nature of the proposed structure enables clear and transparent performance comparisons and this was demonstrated by a comprehensive set of results obtained from closed-loop high fidelity turbine simulations upon a variety of different controller. The proposed control scheme incorporating the knowledge of the upcoming wind and constraints achieved remarkable 43% and 30% reductions in the rotor speed and flap-wise blade moment standard deviations. Additionally, the chance of constraint violations on the rotor speed were significantly down from 2.15% to 0.01%, compared to the baseline controller.

Nonetheless, the performances of the proposed controller were evaluated under assumptions of perfect knowledge of the upcoming wind. Thus, realistic wind measurements with errors and uncertainties could be considered in future work. In addition, the proposed MPC layer design could extend to gain-scheduling feedback controllers addressing the non-linearity of the blade-pitch problem. Furthermore, control designs in below-rated wind conditions were not included in this work, and remain topics of future research.

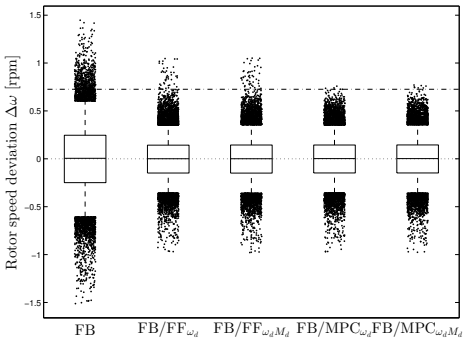

(a) Box plots of the rotor speed deviation. Dash-dot line represents the constraint and dot line denotes the rated speed.

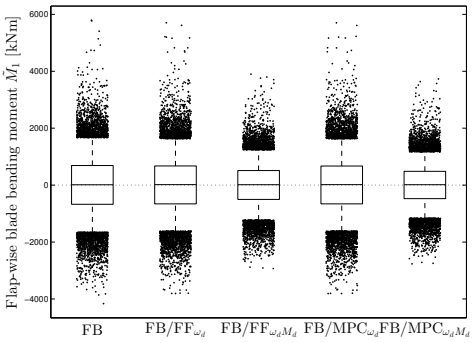

(b) Box plots of the perturbations in flap-wise blade root bending moment of blade 1. Dot line denotes the performance target.

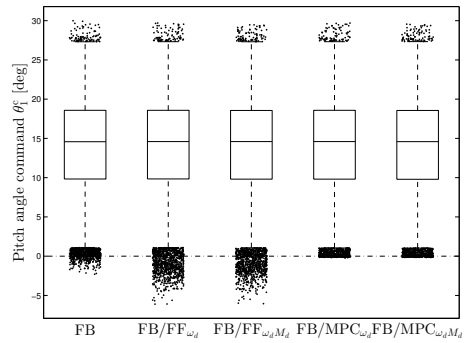

(c) Box plots of the pitch angle command of blade 1. Dash-dot line represents the lower pitch angle constraint.

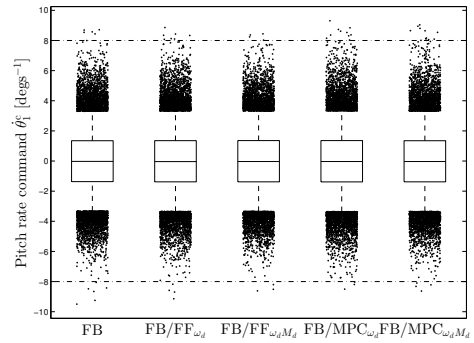

(d) Box plots of pitch rate command of blade 1. Dash-dot lines represent the pitch rate constraints.

Figure 8. Simulation results upon the NREL 5MW turbine under various wind cases with mean wind speed ranging from 13 ms^{-1} to 23 ms^{-1} and turbulence intensity of 14% to 18%, showing the performance comparison between the various controller configurations studied in this paper. Similar results are obtained for the remaining blades.

A. MODEL PARAMETERS AND NOMINAL FEEDBACK CONTROLLERS

The parameters of $G(s)$ and $G_d(s)$ (6) are detailed in Table III and the closed-loop robust controllers (8) are described as follows:

$$K_{\theta\omega}(s) = -\frac{10.74s + 3.85}{3.14s}, \tag{25a}$$

$$K_{\theta M}(s) = -10^{-4} \times \frac{2.28s^4 + 1.93s^3 + 5.87s^2 + 8.79s - 2.51}{s^4 + 0.16s^3 + 7.97s^2 + 0.38s + 10.22}. \tag{25b}$$

Parameters	Values	Units	Parameters	Values	Units
$\frac{d\omega}{d\theta}$	-0.84	$\mathrm{rpm\,deg}^{-1}$	$\frac{dM_{\mathrm{flap}}}{d\theta}$	-1.50×10^6	$\mathrm{Nm\,deg}^{-1}$
τ_{r}	4.00	s	f_{b}	0.70	Hz
D_{b}	0.47	-	τ_{a}	0.11	s
f_{h}	0.80	Hz	f_{l}	0.014	Hz

Table III. Model parameter of $G(s)$ and $G_d(s)$ (6)

Wind Energ. 2010; **00**:1–19 © 2010 John Wiley & Sons, Ltd.
DOI: 10.1002/we
Prepared using weauth.cls

B. DETAILS OF THE MATRICES M_c, M_d AND E

The shift matrices $M_c \in \mathbb{R}^{n_u n_c \times n_u n_c}$ and $M_d \in \mathbb{R}^{n_d n_a \times n_d n_a}$ are defined as follows:

$$M_c = \begin{bmatrix} 0 & I & 0 & \cdots & 0 \\ 0 & 0 & I & \cdots & 0 \\ \vdots & \vdots & \vdots & \ddots & \vdots \\ 0 & 0 & 0 & \cdots & I \\ 0 & 0 & 0 & \cdots & 0 \end{bmatrix}, \; M_d = \begin{bmatrix} 0 & I & 0 & \cdots & 0 \\ 0 & 0 & I & \cdots & 0 \\ \vdots & \vdots & \vdots & \ddots & \vdots \\ 0 & 0 & 0 & \cdots & I \\ 0 & 0 & 0 & \cdots & 0 \end{bmatrix}, \tag{26a}$$

and $E \in \mathbb{R}^{n_x \times n_u n_c}$ are described as follows:

$$E = \begin{bmatrix} I & 0 & 0 & \cdots & 0 \end{bmatrix} \tag{26b}$$

C. PROOF OF THEOREM 1

The proof is based on inspection of (15c). By investigating the cost function (15c), the Lyapunov equation $\Psi^T S \Psi = S - W$ for (15c) can be used and expressed as follows:

$$\begin{bmatrix} \Phi^T & 0 & 0 \\ E^T B^T & M_c^T & 0 \\ E^T B_d^T & 0 & M_d^T \end{bmatrix} \begin{bmatrix} S_x & S_{xc} & S_{xd} \\ S_{xc}^T & S_c & S_{cd} \\ S_{xd}^T & S_{cd}^T & S_d \end{bmatrix} \begin{bmatrix} \Phi & BE & B_d E \\ 0 & M_c & 0 \\ 0 & 0 & M_d \end{bmatrix} - \begin{bmatrix} S_x & S_{xc} & S_{xd} \\ S_{xc}^T & S_c & S_{cd} \\ S_{xd}^T & S_{cd}^T & S_d \end{bmatrix} + \begin{bmatrix} Q + K^T R K & K^T R E & 0 \\ E^T R K & E^T R E & 0 \\ 0 & 0 & 0 \end{bmatrix} = 0. \tag{27}$$

To find the conditions where $S_{xc}^T = 0$, begin from the top-left equality of (27):

$$\Phi^T S_x \Phi - S_x + Q + K^T R K = 0, \tag{28}$$

which forms the first condition of Theorem 1. Note that this is the Lyapunov equation for the pre-determined feedback control law and since $x_{k+1} = \Phi x_k$ where the closed-loop dynamics Φ is asymptotically stable, given any $Q > 0$, there exist a unique $S_x > 0$ satisfying (28). Subsequently, considering the middle-left equality of (27):

$$E^T B^T S_x \Phi + M_c^T S_{xc}^T \Phi - S_{xc}^T + E^T R K = 0, \tag{29a}$$

and since $S_x > 0$, the condition for $S_{xc}^T = 0$ is if and only if :

$$E^T B^T S_x \Phi + E^T R K = 0, \tag{29b}$$

and (29b) can be further simplified:

$$B^T S_x \Phi + R K = 0. \tag{29c}$$

To show $B^T S_x \Phi + RK = 0$ is a necessary and sufficient condition for $S_{xc}^T = 0$, proofs of sufficiency and necessity are provided.

Proof of sufficiency: Suppose $B^T S_x \Phi + RK = 0$ and rewrite 29a as follows:

$$\begin{bmatrix} B^T S_x \Phi \\ 0 \\ \vdots \\ 0 \\ 0 \end{bmatrix} + \begin{bmatrix} 0 & 0 & \cdots & 0 & 0 \\ I & 0 & \cdots & 0 & 0 \\ 0 & I & \cdots & 0 & 0 \\ \vdots & \vdots & \ddots & \vdots & \vdots \\ 0 & 0 & \cdots & I & 0 \end{bmatrix} \underbrace{\begin{bmatrix} S_{xc_{\{1,:\}}}^T \Phi \\ S_{xc_{\{2,:\}}}^T \Phi \\ \ddots \\ S_{xc_{\{n_c-1,:\}}}^T \Phi \\ S_{xc_{\{n_c,:\}}}^T \Phi \end{bmatrix}}_{S_{xc}^T \Phi} - \underbrace{\begin{bmatrix} S_{xc_{\{1,:\}}}^T \\ S_{xc_{\{2,:\}}}^T \\ \ddots \\ S_{xc_{\{n_c-1,:\}}}^T \\ S_{xc_{\{n_c,:\}}}^T \end{bmatrix}}_{S_{xc}^T} + \begin{bmatrix} RK \\ 0 \\ \vdots \\ 0 \\ 0 \end{bmatrix} = 0, \tag{30a}$$

where $S_{xc}^T \in \mathbb{R}^{n_u n_c \times n_x}$ is expressed in terms of $S_{xc_{\{i,:\}}}^T \in \mathbb{R}^{n_u \times n_x}$ for $i \in \{1, \cdots, n_c\}$. Considering the first equality of (30a):

$$B^T S_x \Phi - S_{xc_{\{1,:\}}}^T + RK = 0. \tag{30b}$$

Substituting $B^T S_x \Phi + RK = 0$ into (30b) yields $S_{xc_{\{1,:\}}}^T = 0$. Subsequently, the second equality of (30a) is as follows:

$$S_{xc_{\{1,:\}}}^T \Phi = S_{xc_{\{2,:\}}}^T. \tag{30c}$$

Inserting $S_{xc_{\{1,:\}}}^T = 0$ into (30c) yields $S_{xc_{\{2,:\}}}^T = 0$, irrespective of $\Phi \in \mathbb{R}^{n_x \times n_x}$ being full rank or not. Similarly, examining the subsequent equality of (30a):

$$S_{xc_{\{i,:\}}}^T \Phi = S_{xc_{\{i+1,:\}}}^T, \; i \in \{2, \cdots, n_c - 1\}. \tag{30d}$$

By induction, substituting $S_{xc_{\{i,:\}}}^T = 0$ into (30d) yields $S_{xc_{\{i+1,:\}}}^T = 0$ for $i \in \{2, \cdots, n_c - 1\}$. Consequently, all entries of S_{xc}^T are zeros which implies $S_{xc}^T = 0$, that proves $B^T S_x \Phi + RK = 0$ is a sufficient condition.

Proof of necessity: To demonstrate $B^T S_x \Phi + RK = 0$ is a necessary condition for $S_{xc}^T = 0$, a contradiction argument is used. Suppose $B^T S_x \Phi + RK \neq 0$, based on the equality of (30b), $S_{xc_{\{1,:\}}}^T$ becomes as follows:

$$S_{xc_{\{1,:\}}}^T = B^T S_x \Phi + RK \neq 0. \tag{31}$$

If $S_{xc_{\{1,:\}}}^T \neq 0$, then $S_{xc}^T \neq 0$. Thus, this proves $B^T S_x \Phi + RK = 0$ is a necessary condition for $S_{xc}^T = 0$, which forms the second condition of Theorem 1.

REFERENCES

1. Geyler M, Caselitz P. Robust Multivariable Pitch Control Design for Load Reduction on Large Wind Turbines. *Journal of Solar Energy Engineering* 2008; **130**.
2. Selvam K, Kanev S, van Wingerden JW, van Engelen T, Verhaegen M. Feedback-feedforward individual pitch control for wind turbine load reduction. *International Journal of Robust and Nonlinear Control* 2009; **19**(1):72–91.
3. Leithead W, Neilson V, Dominguez S. Alleviation of Unbalanced Rotor Loads by Single Blade Controllers. *European Wind Energy Conference*, 2009.
4. Kodama N, Matsuzaka T, Tuchiya K, Arinaga S. Power variation control of a wind generator by using feed forward control. *Renewable Energy* 1999; **16**:847–850.
5. Harris M, Hand M, Wright A. Lidar for Turbine Control. *Technical Report* 2005.
6. Schlipf D, Fischer T, Carcangiu C. Load analysis of look-ahead collective pitch control using LIDAR. *Proc. of 10th German Wind Energy Conference*, 2010.
7. Bossanyi EA, Kumar A, Hugues-Salas O. Wind turbine control applications of turbine-mounted LIDAR. *The Science of Making Torque from Wind*, 2012.
8. Dunne F, Pao L, Wright A, Jonkman B, Kelley N, Simley E. Adding Feedforward Blade Pitch Control for Load Mitigation in Wind Turbines: Non-Causal Series Expansion, Preview Control, and Optimized FIR Filter Methods. *Proc. of 49th AIAA*, 2011.
9. Schlipf D, Schuler S, Grau P, Martin K. Look-Ahead Cyclic Pitch Control Using LIDAR. *The Science of Making Torque from Wind*, 2010.
10. Laks J, Pao L, Wright A, Kelley N, Jonkman B. The use of preview wind measurements for blade pitch control. *Mechatronics* 2011; **21**(4):668–681.
11. Wang N, Johnson KE, Wright AD, Wright AD. FX-RLS-based feedforward control for LIDAR-enabled wind turbine load mitigation. *IEEE Transactions on Control Systems Technology* 2012; **20**(5):1212–1222.
12. Dunne F, Pao LY, Wright AD, Jonkman B, Kelley N. Adding feedforward blade pitch control to standard feedback controllers for load mitigation in wind turbines. *Mechatronics* 2011; **21**:682–690.
13. Kumar A, Stol K. Scheduled model predictive control of a wind turbine. *Proc. of AIAA/ASME Wind Energy Symp*, 2009.
14. Soliman M, Malik OP, Westwick DT. Multiple Model Predictive Control for Wind Turbines With Doubly Fed Induction Generators. *IEEE Transactions on Sustainable Energy* 2011; **2**(3):215–225.
15. Henriksen L, Hansen M, Poulsen N. Wind turbine control with constraint handling: a model predictive control approach. *IET Control Theory & Applications* 2012; **6**(11):1722.

DOI: 10.1002/we
Prepared using weauth.cls

16. Hur S, Leithead WE. Model predictive and linear quadratic Gaussian control of a wind turbine. *Optimal Control Applications and Methods* 2016; **143**.
17. Laks J, Pao L, Simley E, Wright A, Kelley N, Jonkman B. Model Predictive Control Using Preview Measurements From LIDAR. *49th AIAA*, American Institute of Aeronautics and Astronautics: Reston, Virigina, 2011.
18. Spencer MD, Stol KA, Unsworth CP, Cater JE, Norris SE. Model predictive control of a wind turbine using short-term wind field predictions. *Wind Energy* 2013; **16**(3):417–434.
19. Mirzaei M, Soltani M. Model predictive control of wind turbines using uncertain LIDAR measurements. *Proc. of the American Control Conference* 2013; :2235–2240.
20. Körber A, King R. Nonlinear Model Predictive Control for Wind Turbines. *Ewea*, 2011; 1–6.
21. Schlipf D, Schlipf DJ, Kühn M. Nonlinear model predictive control of wind turbines using LIDAR. *Wind Energy* 2013; **16**(7):1107–1129.
22. Lio WH, Rossiter J, Jones BL. A review on applications of model predictive control to wind turbines. *2014 UKACC International Conference on Control (CONTROL)*, IEEE: Loughborough, U.K., 2014; 673–678.
23. Rezaei V. Advanced control of wind turbines: Brief survey, categorization, and challenges. *2015 American Control Conference (ACC)*, IEEE, 2015; 3044–3051.
24. Bossanyi EA. Individual Blade Pitch Control for Load Reduction. *Wind Energy* 2003; **6**(2):119–128.
25. Lu Q, Bowyer R, Jones B. Analysis and design of Coleman transform-based individual pitch controllers for wind-turbine load reduction. *Wind Energy* 2015; **18**(8):1451–1468.
26. Towers P, Jones BL. Real-time wind field reconstruction from LiDAR measurements using a dynamic wind model and state estimation. *Wind Energy* 2016; **19**(1):133–150.
27. Raach S, Schlipf D, Haizmann F, Cheng PW. Three Dimensional Dynamic Model Based Wind Field Reconstruction from Lidar Data. *The Science of Making Torque from Wind*, 2014.
28. Zhang Y, Cheng M, Chen Z. Proportional resonant individual pitch control for mitigation of wind turbines loads. *IET Renewable Power Generation* 2013; **7**(3):191–200.
29. Lio WH, Jones BL, Lu Q, Rossiter J. Fundamental performance similarities between individual pitch control strategies for wind turbines. *International Journal of Control* 2015; :1–16.
30. Rossiter JA, Kouvaritakis B, Rice MJ. A numerically robust state-space approach to stable-predictive control strategies. *Automatica* 1998; **34**(1):65–73.
31. Rossiter JA. *Model-Based Predictive Control: A Practical Approach*. CRC Press, 2003.
32. Scokaert POM, Rawlings JB. Feasibility issues in linear model predictive control. *AIChE Journal* 1999; **45**(8):1649–1659.
33. Gilbert E, Tan K. Linear systems with state and control constraints: the theory and application of maximal output admissible sets. *IEEE Transactions on Automatic Control* 1991; **36**(9):1008–1020.
34. Boyd S, El Ghaoui L, Feron E, Balakrishnan V. *Linear Matrix Inequalities in System and Control Theory*. Society for Industrial and Applied Mathematics, 1994.
35. Jonkman J, Butterfield S, Musial W, Scott G. Definition of a 5-MW Reference Wind Turbine for Offshore System Development. *Technical Report*, National Renewable Energy Laboratory (NREL), Golden, CO 2009.
36. Jonkman J, Buhl Jr M. FAST User's Guide. *Technical Report*, National Renewable Energy Laboratory (NREL) 2005.
37. Jonkman B. TurbSim User's Guide. *Technical Report*, National Renewable Energy Laboratory (NREL) 2009.
38. Rossiter JA, Grinnell BG. Improving the tracking of generalized predictive control controllers. *Journal of Systems and Control Engineering*, vol. 210, 1996; 169–182.